Article
Vol. 23, No. 3, p. 391–408, June 2019
https://doi.org/10.1007/s12303-018-0057-5
pISSN 1226-4806 eISSN 1598-7477
Geosciences Journal GJ

The exhumation along the Kenyase and Ketesso shear zones in the Sefwi terrane, West African Craton: a numerical study

Xiaojun Feng[1,2]*, Enyuan Wang[1], Jérôme Ganne[2], Roland Martin[2], and Mark Jessell[2,3]

[1]School of Safety Engineering, China University of Mining and Technology, Xuzhou 221116, China
[2]Geosciences Environnement Toulouse, Observatoire Midi Pyrénées, Toulouse 31400, France
[3]Centre for Exploration Targeting, The University of Western Australia, Perth WA 6009, Australia

ABSTRACT: High-grade (amphibolite–granulite facies) tectono-metamorphic domains in the Sefwi terrane of Ghana are separated from adjacent lower-grade (greenschist facies) greenstone belts by two main shear zones. The high-grade rocks presumably exhumed along the sinistral shear zones during the D2 ENE-WSW transtension (~2073 Ma). To better understand the role boundary conditions and the spatial relationship of faults play in the exhumation of partially molten lower crust in the Sefwi terrane, ten 3D thermo-mechanical models have been constructed. The results show that the normal component of velocity boundary conditions mainly controls the exhumation (8–10 km) of the lower crust along pre-existing faults, while the exhumation in the relay zones between faults is controlled by the obliquity between the applied extensional velocity vector and the vertical wall on which it is applied. The strike of the exhumation belt made of partially molten lower crust rocks in the relay zone is sub-orthogonal to the horizontal maximum stretching axis. The isostatic compensation from low-density upper mantle to overlying crust (thinning) is higher under transtension than under extension. The lower crust exhumation influenced by inherited shear zones (ductile) can be used to better understand the loci of the high-grade rocks in the Sefwi terrane. We suggest that the Kukuom-Juaboso domain composed of amphibolite–migmatite facies rocks probably resulted from the concentration of partially molten rocks in the relay zone between the Ketesso and Kenyase shear zones during the D2 ENE-WSW transtension. The two shear zones probably underwent two main stages for growth and maturation from the D1 to D2 phases. The regional exhumation of the high-grade rocks in the Sefwi terrane probably occurred within < 5 Ma.

Key words: numerical modelling, Eburnean Orogeny, deformation, strike-slip faults, West African Craton

Manuscript received May 30, 2018; Manuscript accepted September 3, 2018

1. INTRODUCTION

Pre-existing faults commonly act as preferentially re-activated sites when external boundary conditions change (Chester et al., 1991; Misra and Mukherjee, 2015), and play a dominant role in concentrating high strain (Morley et al., 2004) temporally. A regional-scale fault commonly originates from a network of local pre-existing discontinuities, through which fracture propagation of their surrounding rocks will be inhibited (Teufel and Clark, 1984). With respect to an interacting strike-slip fault system (e.g., Dasgupta and Mukherjee, 2017), both soft and hard linkages are commonly involved. During the growth and propagation of faults, a soft linkage can mature to a hard linkage via fracture propagation at the tips of faults and repeated interaction between faults (Gupta and Scholz, 2000; Pachell and Evans, 2002).

The emplacement of partially molten rocks into upper/middle crust is dominantly driven by the contrasts in density compared to surrounding solid rocks (Brown, 1994; Petford et al., 2000; Mukherjee and Mulchrone, 2012). Pre-existing faults are thought to play an important role in influencing and promoting the processes of the emplacement (Koyi and Skelton, 2001; Tirel et al., 2008). For extension-dominated regional exhumation of the lower crust, Feng (2016c) demonstrated that the orientation of pre-existing faults largely controls the rate and distribution of lower crust exhumation using 2D and 3D thermo-mechanical models. The influence of pre-existing faults on the formation

*Corresponding author:
Xiaojun Feng
School of Safety Engineering, China University of Mining and Technology, Xuzhou 221116, China
Tel: +86-516-8388-4695, E-mail: xiaojun.feng@cumt.edu.cn

process of metamorphic core complexes (MCCs) during extension has also been explored in analogue models (Koyi and Skelton, 2001), and the structural evolution coincides well with numerical results (Tirel et al., 2008).

The growth of a fault system under transtensional boundary conditions has been widely studied (Fossen and Tikoff, 1998; Lin et al., 1998; Dooley and Schreurs, 2012). Furthermore, the exhumation of high grade rocks simulated by numerical and analogue models has been also explored under compressional (Lin et al., 2000; Ganne et al., 2014), extensional (Brun et al., 1994) and Poiseuille flow (Mukherjee et al., 2012) boundary conditions. However, 3D numerical models including the processes of fault growth and lower crust exhumation driven by transtension boundary conditions have still not been completely explored.

The Sefwi terrane of SW Ghana is mainly composed of the North-Western Sunyani basin, the South-Eastern Kumasi basin and the central high-grade Kukuom-Juaboso domain (KJD). The KJD is bounded by two main NE trending shear zones (150–250 km long): the Kenyase shear zones to the Northwest and the Ketesso shear zones to the Southeast.

To better understand how the spatial distribution of these two shear zones and boundary conditions influence the regional exhumation of the partially molten lower crustal rocks, ten 3D thermo-mechanical models have been explored. The models are constrained by the metamorphic rock records (P-T paths) within the study area and structural interpretation (distribution of different rocks as a result of shear zones) performed by McFarlane et al. (2016), McFarlane (2018) and Jessell et al. (2012). This study may shed light on the role high strain zones play in exhumation of partially molten lower crust under transtension

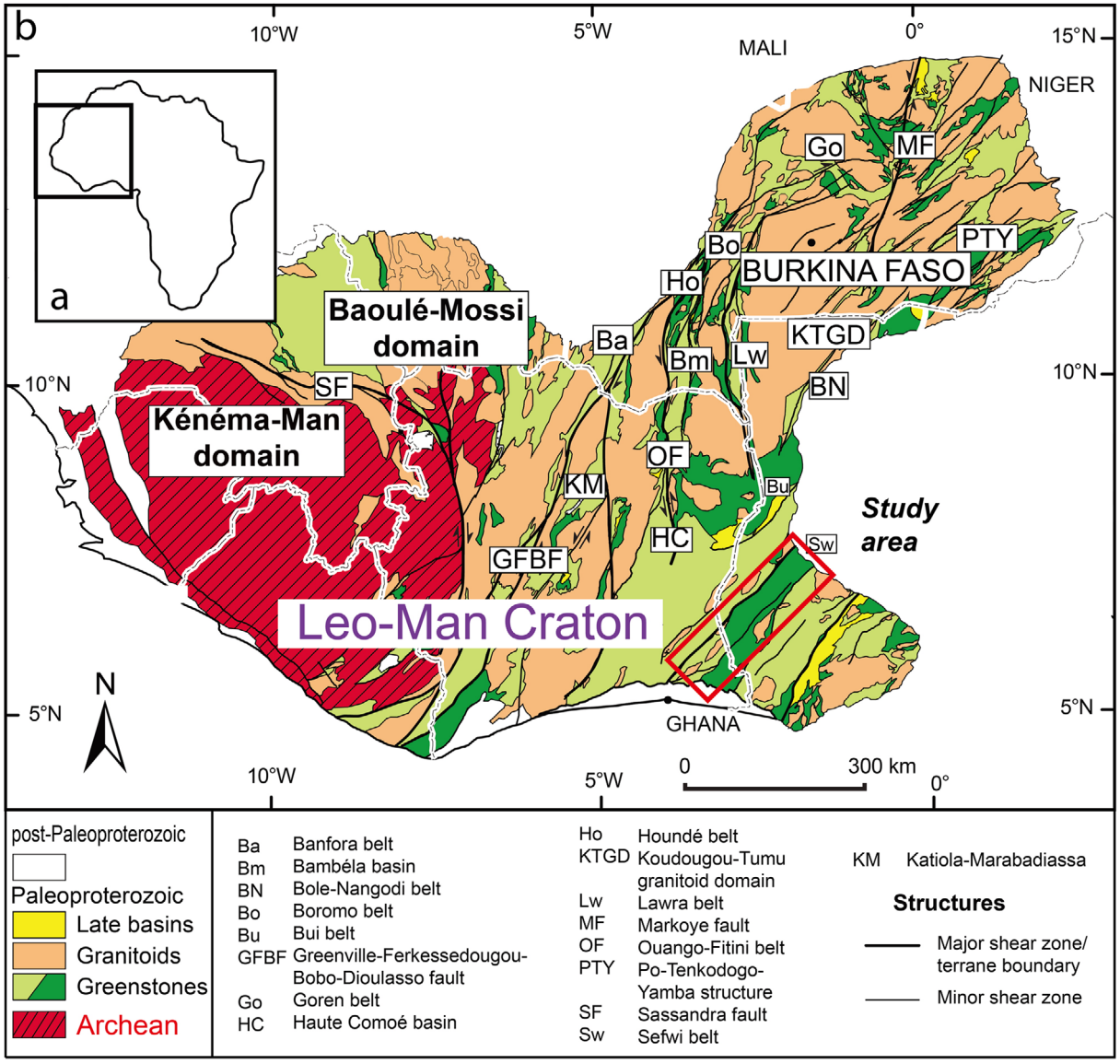

Fig. 1. Geological map of the Leo-Man Craton of the WAC after Milési et al. (2004). It shows major shear zones and Paleoproterozoic–Archaean blocks. The Ghanaian Sefwi domain is indicated by a red box, a detailed metamorphic and structural map can be found in Figure 2.

boundary conditions, as well as on the evolution of structures and deformation in the Sefwi terrane during the Eburnean Orogeny (ca. 2.2–2.0 Ga).

2. GEOLOGY

The Leo-Man Craton (Fig. 1) is the southernmost segment of the West African Craton (WAC). It is composed of the Eastern Paleoproterozoic Baoul-Mossi (BM) domain and the South-Western Archaean Kénéma-Man (KM) domain. These two domains are separated by the Sassandra Fault (SF). The KM domain consists of the oldest gneissic rock (3600–3500 Ma, U/Pb zircon dating) in the WAC (Rollinson, 2016). The ages of major rocks range 3026 and 2850 Ma (U/Pb zircon dating). This domain was mainly intruded by two episodic magmatic pules, one between 3260 and 3050 Ma and the other between 2960 and 2850 Ma (Rollinson, 2016). The BM domain consists of extensively distributed NS trending greenstone-granitoid belts (Fig. 1b). The intruded granitoids in the BM domain locally yield ages between 2195 and 2172 Ma (Hirdes et al., 1992; Baratoux et al., 2011). Several generations of main magmatic pulses took place later, ranging between 2153 and 2068 Ma (U/Pb zircon dating; Gasquet et al., 2003; Baratoux et al., 2011; Block et al., 2015).

The Sefwi-Sunyani-Como region (Fig. 1b, outlined by red box) is in South-Western Ghana and the Ivory Coast, and consists of several sub-parallel NE-SW trending greenstone belts (the maximum length: 600–700 km). The Sunyani and Kumasi basins (Fig. 2) are mainly comprised of volcaniclastics, wackes and argillites (Leube et al., 1990). The two basins were intruded by numerous granitoids with crystallization ages of 2088 ± 1 Ma for the Sunyani basin and 2116 ± 2 Ma (U/Pb zircon dating) for the Kumasi basin, respectively (Hirdes et al., 1992). The Sefwi greenstone belt is composed of metamorphosed tholeiitic lavas, volcanoclastic and granitoids (Agyei duodu et al., 2009). The intruded granitoids within the belt yield ages of about 2180–2170 Ma (U/Pb zircon dating, Hirdes et al., 1992).

The high grade tectono-metamorphic KJD of up to amphibolite–migmatite facies is bounded by the Kenyase and Ketesso shear

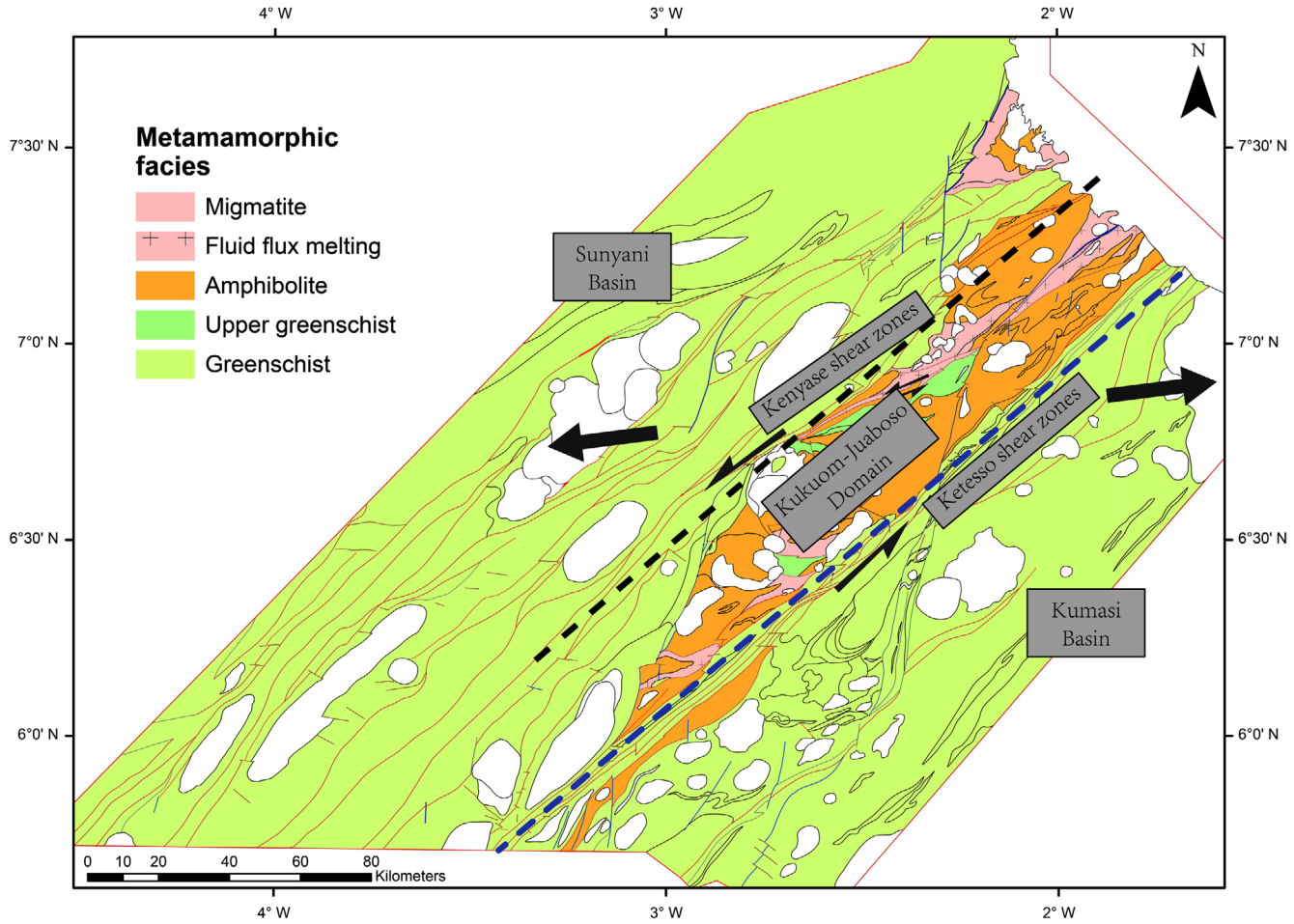

Fig. 2. Metamorphic map of the Sefwi terrane of SW Ghana after McFarlane (2018). The D2 deformation stage was dominated by the D2 ENE-WSW transtension (indicated by black arrows). The high grade KJD is bounded by two shear zones: the Kenyase shear zones and the Ketesso shear zones (indicated by black and blue dotted lines).

https://doi.org/10.1007/s12303-018-0057-5

zones (Fig. 2). The Kenyase shear zones mark the boundary between the high grade KJD and the Sunyani basin. The Ketesso shear zones cross through the Sefwi terrane. They separate lower grade domains of greenschist to non-metamorphosed facies in the Kumasi Basin from high grade domains in the Sefwi belt (Feybesse et al., 2006). According to the metamorphic results and structural interpretation performed for the Sefwi terrane by McFarlane et al. (2016), the D1 tectono-metamorphic event contributing to crustal thickening buried crustal rocks up to 10–12 kbar (corresponding to a maximum buried depth about 30–40 km if lithostatic pressure is assumed) and 700–800 °C. The D2 deformation phase was a decompressional stage that took place at about 2073 Ma (McFarlane et al., 2016), through which P-T values decreased to 7–8 kbar (corresponding to a maximum buried depth of about 20–25 km) and 650–700 °C, respectively.

3. METHOD AND MODEL SETUP

The exhumation of lower crust is simulated in a 3D Cartesian geometry using a visco-plastic rheology with the numerical code Underworld (bleeding edge version, Moresi et al., 2003, 2007). The code uses a Lagrangian PIC finite element scheme. The governing mass, momentum and energy conservation equations are solved under the Underworld standard modelling framework, which is expressed as follows (Moresi et al., 2003, 2007):

$$\frac{\partial \sigma_{ij}}{\partial x_j} = \rho_{eff} \cdot g_i \,, \tag{1}$$

$$\nabla \cdot u = 0 \,, \tag{2}$$

$$\frac{\partial T}{\partial t} + u \cdot (\nabla T) = k\nabla^2 T + \frac{H}{Cp} - \frac{lh}{Cp} \cdot \frac{\partial M}{\partial t} \,, \tag{3}$$

where σ_{ij} is the Cauchy stress tensor, g_i is the gravitational acceleration, ρ_{eff} is the effective density, u is the velocity, k is the thermal diffusivity, H is the radiogenic heat production per mass unit, Cp is the heat capacity, lh is the latent heat of fusion and M is the melt fraction.

The 3D model domain is 300 km long (x direction), 140 km wide (y direction) and 60 km thick (z direction, vertical), and modelled with a resolution of 2 km × 2 km × 1 km (Fig. 3). The model is comprised of 16 km thick upper volcano-sediment (it is a genera, and will be compared with prototype), 16 km thick middle crust (mafic), 10 km thick lower crust and 18 km thick upper mantle (from top to bottom, Fig. 3). In the sedimentary and middle crustal domains, two parallel vertical faults are placed. To explore the role that spatial relationship of pre-existing faults plays in the exhumation of the lower crust, two different patterns of fault system (with or without a hexahedral overlapping zone between faults, corresponding to Models A and B shown in Fig. 3) are tested in this study. According to the ratio of extension rate to shear rate applied on the boundaries (0.25~∞; McFarlane et al., 2016; McFarlane, 2018), ten 3D thermo-mechanical

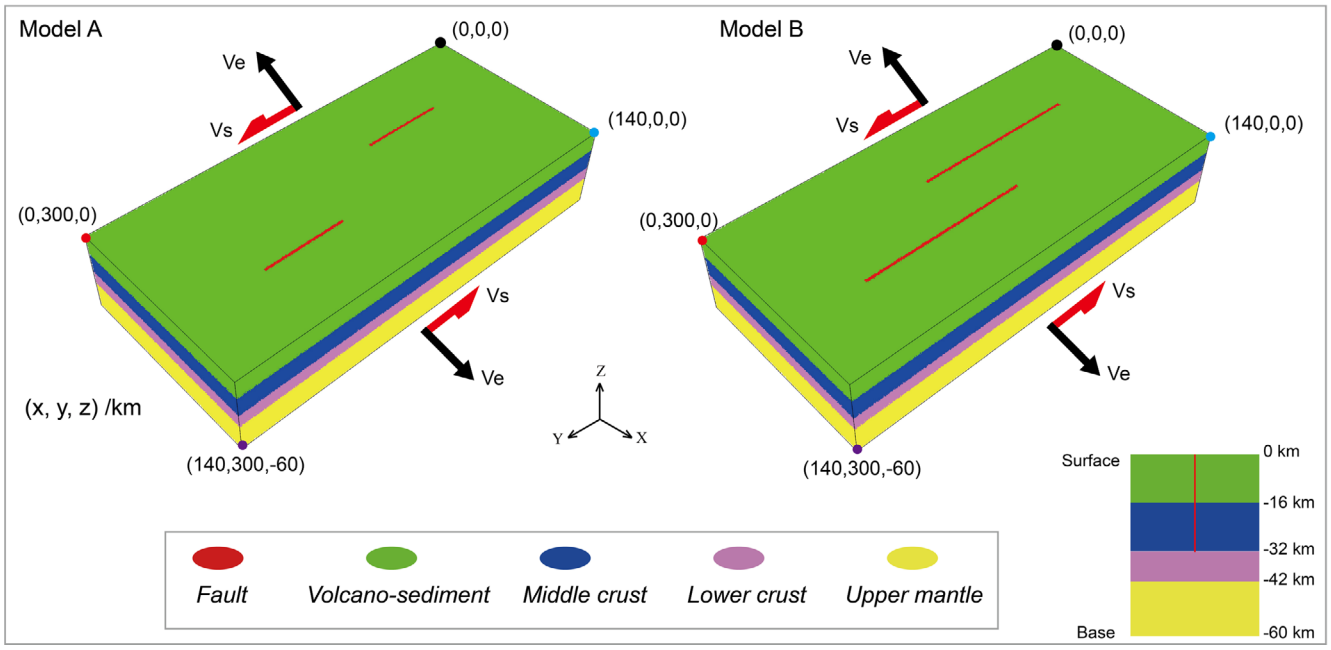

Fig. 3. 3D numerical models are built with the numerical code Underworld (Moresi et al., 2003, 2007). The mechanical boundary conditions are indicated by black and red arrows. Two interacting vertical faults with a thickness of 2 km (Le Pourhiet et al., 2004) are initialized in Models A and B (red colour). The difference between Models A and B is in the spatial relationship between faults (with or without an overlapping zone between two parallel faults). 450 passive particles divided into two groups are placed in the upper surfaces of the lower crust (Z = –32 km) and the upper mantle (Z = –42 km), respectively.

Table 1. Experiments with different parameters on boundary conditions

Pattern	Exp#	Extension rate (*Ve*, cm/year)	Shear rate (*Vs*, cm/year)	*Ve*/*Vs*	Von Mises strain[(a)] (ε_{eq})	Normalized /year (10^{-6})
Model A	A1	2	0	∞	0.09	0.10
	A2	2	1	2	0.10	0.13
	A3	2	2	1	0.16	0.19
	A4	1	2	0.5	0.28	0.17
	A5	1	4	0.25	0.51	0.33
Model B	B1	2	0	∞	0.08	0.10
	B2	2	1	2	0.11	0.13
	B3	2	2	1	0.16	0.19
	B4	1	2	0.5	0.29	0.17
	B5	1	4	0.25	0.41	0.33

[(a)]The Von Mises equivalent strain is calculated by: $\varepsilon_{eq} = \frac{2}{3}\sqrt{\frac{3(e_{xx}^2+e_{yy}^2+e_{zz}^2)}{2}+\frac{3(\gamma_{xy}^2+\gamma_{yz}^2+\gamma_{zx}^2)}{4}}$.

Table 2. Thermo-mechanical model parameters, symbol and value-units

Parameter		Symbol	Value-units
Thickness	Volcano-Sediment	H_{sed}	16 km
	Middle crust	H_{mid}	16 km
	Lower crust	H_{low}	10 km
	Upper mantle	H_{mantle}	18 km
Density	Volcano-Sediment	ρ_{sed}	2800 kg/m^3
	Middle crust	ρ_{mid}	3050 kg/m^3
	Lower crust	ρ_{low}	2700 kg/m^3
	Upper mantle	ρ_{mantle}	3250 kg/m^3
	Pre-existing faults	ρ_{fault}	2750 kg/m^3
Melting point of the lower crust		T	T_{sol} = 636 °C (1%), T_{liq} = 1200 °C (80%)
Heat capacity		Cp	1000 J/kg·K
Thermal diffusivity		k	10^{-6} m^2/s
Latent heat of fusion		lh	250 KJ·kg^{-1}·K^{-1}
Dislocation creep power law pre-exponential factor		A	MPa^{-n}/ s
Dislocation creep power law exponent		n	–
Creep power law activation energy		Q	KJ/mol
Gas constant		R	8.314 J·mol^{-1}·K^{-1}
Gravitational acceleration		g	9.81 m/s^2
Friction angle for Drucker-Prager criterion		φ/f	3–25°
Cohesion for Drucker-Prager criterion		δ_c	3–15 MPa

models (with two classes, Models A and B) are designed for test cases (boundary conditions in Tables 1 and 2).

Under the PIC finite element frame of the code Underworld, 30 particles are initialized in each cell. To show the exhumation of the lower crust and the compensation from the upper mantle to the overlying crust (crustal thinning during extension), 450 passive particles were employed to trace the changes of position and vertical velocity during transtension (extension). The particles are divided into two groups: one placed in the upper surface of the lower crust (Z = –32 km) and the other one placed in the upper surface of the upper mantle (Z = –42 km).

The mechanical boundaries are constrained by transtension (or extension) with YY-directed periodic boundary conditions (Fig. 3). The bottom of the model considers a free-slip boundary condition. The top surface of the model is a free surface and its boundary thus directly corresponds to the topography (Moresi et al., 2003; Feng et al., 2016a). To balance the volume reduction due to applied extension rate, the upper mantle is allowed to flow in with a normal velocity during extension/transtension (Ganne et al., 2014). With respect to the constraints on thermal boundary conditions, we here model the extension and transtension of a "hot" lithosphere, with a Moho temperature of 840 °C (Tirel et al., 2004). We use fixed temperatures of 0 °C for the model surface and 1200 °C for the base of the model, assuming a fixed

https://doi.org/10.1007/s12303-018-0057-5

temperature gradient of 20 °C/km (Ganne et al., 2012). The solid-deformation behaviour is modelled with a depth-dependent yielding criterion (Drucker and Prager, 2013), which is expressed as follows (Moresi et al., 2007; Sharples et al., 2015):

$$\tau_{II} = \delta_c + P \cdot tan\varphi\,, \tag{4}$$

where τ_{II} is the second invariant of the deviatoric stress tensor, δ_c is the effective cohesion of rocks, P is the local pressure, tanφ is the effective friction coefficient of rocks. In the crustal domain, an initial cohesion value of 15 MPa and an initial coefficient of internal friction angle of 0.3 are defined (Mukherjee, 2017a). The effective cohesion and coefficient of internal friction angle (drop to a maximum of 20% of the initial value when the accumulated strain reaches 0.5, Faulkner et al., 2010) is modelled by coupling with a strain weakening principle (Gueydan et al., 2014; Feng et al., 2016b). The cohesion and coefficient of internal friction angle of pre-existing faults are set to 10% of the initial values of the crust (as per Rey et al., 2009).

According to the metamorphic modelling calculated by Ganne et al. (2014), the mafic crust rocks start to melt (from 1% to 30 %) at a solidus temperature of ~836 °C (corresponding to a buried depth of ~42 km at the given temperature gradient of 20 °C/km). In this study, the middle crust layer is placed between Z = –16 km and Z = –32 km (Fig. 3, Table 3). Under extension (transtension) boundary conditions, the upper crust hardly melts. We therefore only allow the lower crust to undergo partial melting process. We assume that the T_{sol} and T_{liq} temperatures of the lower crust do not change with pressure/depth (Gerya et al., 2008; Ganne et al., 2014). To calculate the volumetric melt fraction (M), the volumetric melting coefficient (X_M) for calculating melt fraction (M) is introduced as follows (Gerya et al., 2008):

$$X_M = 0 \quad \text{at } T \le T_{sol}\,,$$

$$X_M = \frac{T - T_{sol}}{T_{liq} - T_{sol}} \quad \text{at } T_{sol} < T < T_{liq}\,,$$

$$X_M = 1 \quad \text{at } T \ge T_{liq}\,, \tag{5}$$

where T_{sol} and T_{liq} represent the wet solidus and dry liquidus temperatures of the lower crust, respectively.

We assume that the volumetric melt fraction (M) increases linearly, when the temperature is above the wet solidus temperature and below the dry liquidus temperature (Gerya et al., 2008; Ganne et al., 2014).

$$M = X_M \cdot M_{max}\,. \tag{6}$$

In natural cases, the effective viscosity of partially molten rocks is usually 10^3~10^{10} times lower than their surrounding solid rocks (Vanderhaeghe, 2001; review in Mukherjee, 2013). In our models, When the lower crust reaches its solidus (T_{sol}), its effective viscosity changes according to a function of melt fraction (M) (Pinkerton and Stevenson, 1992):

$$\eta_{eff} = 5 \times 10^{16} \cdot \exp\left(2.5 + (1 - M)\left(\frac{1 - M}{M}\right)^{0.48}\right). \tag{7}$$

The effective density in the model domain is calculated according to the local temperature, the thermal expansion coefficient (α) of $3{\cdot}10^{-5}$ (1/K) and the melt fraction (M). Density can also change spatially and in that case also effective density is calculated (Mukherjee, 2017b, 2018a). For rocks which cannot melt, a linear relationship used for calculating effective density is expressed as Equation (8). For the lower crust layer, the effective density is calculated by Equation (9), which is similar to the equations employed in Rey et al. (2009):

$$\rho_{eff} = \rho[1 - \alpha \cdot (T - T_0)]\,, \tag{8}$$

$$\rho_{eff} = \rho[1 - \alpha \cdot (T - T_0) - \beta \cdot M]\,, \tag{9}$$

where ρ_{eff} is the effective density, α is the coefficient of thermal expansion, T is the local temperature, T_0 is the reference temperature at top surface (0 °C), β is the coefficient of expansion related to phase change.

4. RESULTS

We have constructed ten 3D thermo-mechanical models (with two classes, Models A and B, with detailed parameters about the boundary conditions can be found in Table 1 and Fig. 3) to explore the influence of pre-existing faults on exhumation of partially molten lower crust during extension and transtension. All simulations were run in parallel on the EOS cluster machine in Toulouse, France (https://www.calmip.univ-toulouse.fr/).

Table 3. Rheological parameters employed for modelling different lithospheric layers are collected from Ranalli (1995)

Layer	Rock type	A (MPa^{-n}/s)	n	Q (KJ/mol)
Volcano-Sediment	Wet quartzite	3.2×10^{-4}	2.3	154
Middle crust	Diabase	2.0×10^{-4}	3.4	260
Lower crust	Quartzodiorite	1.3×10^{-3}	2.4	219
Upper mantle	Dry olivine	7×10^{4}	3.3	520
Pre-existing fault		Initial viscosity (10^{20} Pa s)		

The effective viscosity is calculated with a non-Newtonian power law using the equation: $\eta_0 = 0.25 \cdot (0.75A)^{(-1/n)} \cdot \dot{\varepsilon}^{((1/n)-1)} \cdot \exp^{(Q/nRT)}$.

4.1. The Upper Surface of the Partially Molten Lower Crust

Initially, we applied a fixed extension rate of 2 cm/year in X direction (Fig. 3) on the boundaries for experiments A1 and B1 (Figs. 4A1 and 4B1). The results show that the partially molten lower crust rocks concentrate preferentially along pre-existing faults during extension. In the relay zone between faults, the concentration of the partially molten lower crustal materials is much lower than that along the faults. Comparing cases A1 with B1, the focus of exhumation in relay zones between faults in case A1 (6–8 km exhumed height) is higher than that in case B1 (4–5 km exhumed height).

In experiments A2 and B2, a tangential component of velocity boundary conditions was additionally introduced into the fault system. The ratio of extension rate to shear rate applied on the boundaries was set to 2, which means that this fault system is still dominated by the applied normal component of velocity boundary conditions. For case A2 (Fig. 4A2), the partially molten lower crust rocks move towards the faults and their overlapping zone, leading to the formation of a exhumed belt (red in Fig. 4A2, reaching about 10 km of uplift) made of partially molten rocks. While case B2 (Fig. 4B2) only shows a high concentration of the partially molten lower crust rocks along the faults. At about 0.88 Ma (from the start of the model), the upper surface of the partially molten lower crust in case B2 reaches about 10 km of uplift along the faults and only 5–7 km of uplift in their relay zone.

In experiments A3 and B3, we further increased the shear rate in the fault system, making it equal to extension rate applied on boundaries. Case A3 (Fig. 4A3) shows that a high concentration of the lower crust exhumation is observed both along the faults and in the relay zone between faults. Compared to case A2, the relay zone in case A3 concentrates much more partially molten rocks (about 1.1 times of the width of the exhumed belt). Regarding the exhumation along the faults in case B3 (Fig. 4B3), which shows a very similar distribution of the lower crust with cases B1 and B2. While the exhumation occurred around the relay zone in case B3, it is largely increased compared to cases B1 and B2. The difference in the distribution of the lower crust exhumation indicates that increasing the shear rate to the value of extension rate applied can enhance the concentration of the partially molten lower crust in the relay zone between faults during transtension.

Further increasing the shear rate in experiments A4 and B4 (making the ratio of extension rate to shear rate equal 0.5) results in the tangential component of velocity boundary conditions becomes dominant in the fault system. Case A4 shows that the branch of the red exhumation belt located into the relay zone is wider than its other red branches along the faults (Fig. 4A4). Regarding case B4 (Fig. 4B4), it shows that the distribution of the lower crust exhumation is similar to case B3. Highly concentrated partially molten rocks in the relay zone link the uplifted partially molten rocks along the faults.

In experiments A5 and B5, the ratio of extension rate to shear rate applied on boundaries was decreased to 0.25, and the tangential component of velocity boundary conditions dominates compared to other experiments (A1–A4, B1–B4). The results show that the distribution of the exhumation in cases A5 and B5 is characterized by a relatively high concentration of partially molten lower crust rocks along two parallel high strain zones and a relatively low concentration of the exhumation in the relay zone. The two parallel high strain zones originated from the two pre-existing faults develop well and mature during transtension (white dotted lines in Figs. 4A5 and 4B5).

Comparing all the experiments, the results show that the normal component of velocity boundary conditions generally controls the exhumation of the partially molten rocks occurred along faults, while the exhumation of the lower crust in the relay zone between faults is pre-dominated by the ratio of extension rate to shear rate applied on boundaries. With respect to the exhumation of the lower crust occurred in the relay zone between faults, its concentration generally increases with the decreasing ratio of extension rate to shear rate to an extent (experiments A1–A4 and B1–B4).

4.2. Surface Relief

At a crustal scale, faulting and lower crust exhumation shape the surface relief (Feng et al., 2016a). In an extensional setting (Figs. 5A1 and 5B1), the relay zone between faults in case A1 shows a subsidence of about 1–1.5 km, while in case B1 it shows about 2 km of uplift at 0.85 Ma.

In transtension, experiments A2–A4 show a generally similar distribution of relief with each other (Figs. 5A2, 5A3 and 5A4). Subsidence (green colour) mainly focuses along faults and in the relay zone between faults, forming a continuous subsidence belt. The width of the subsidence belt in the relay zone increases with the decreasing ratio of extension rate to shear rate applied (the ratio decreases by the order: A1-A2-A3-A4). Regarding the distribution of uplift, cases A1 and A2 show focused uplift along the SE and NW edges of the subsidence region. The uplifted region observed in experiments A3 and A4 also focus along the edges of the subsidence belts, but it distributes in a generally even fashion compared to experiments A1 and A2. For experiments B1–B4, the subsidence region in the relay zone between faults widens with the decreasing ratio of extension rate to shear rate (from experiments B1 to B4), while the distribution of the uplifted region is similar with each other.

https://doi.org/10.1007/s12303-018-0057-5

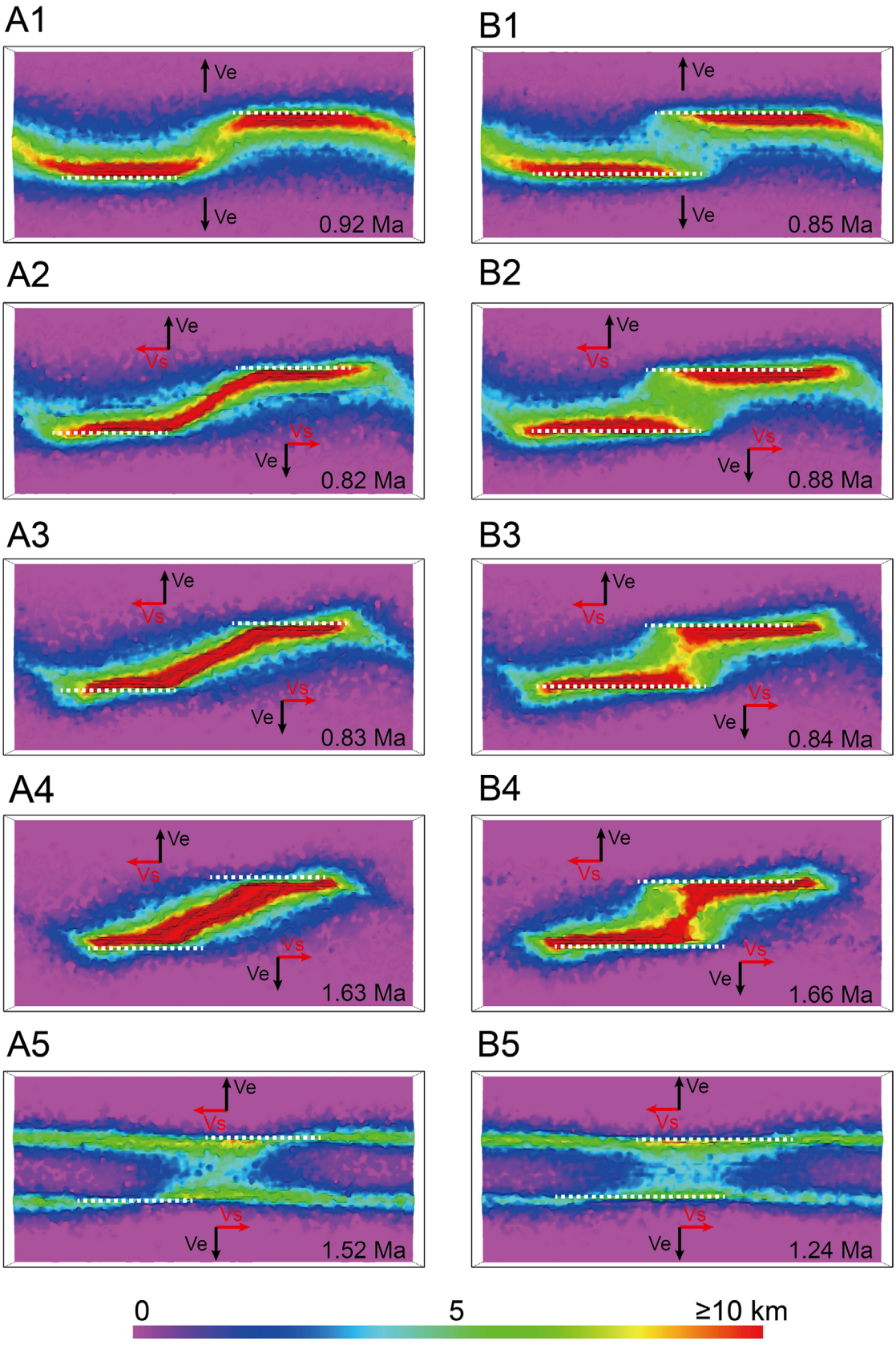

Fig. 4. The relief of the upper surface of the partially molten lower crust in extension (experiments A1 and B1) and transtension (experiments A2–A5 and B2–B5). The first and second columns correspond to the different standard models: Models A and B (Fig. 3), respectively. Pre-existing faults are indicated in white dotted lines. Boundary conditions are indicated by black and red arrows. The colour bar represents the exhumation of the partially molten lower crust during extension and transtension.

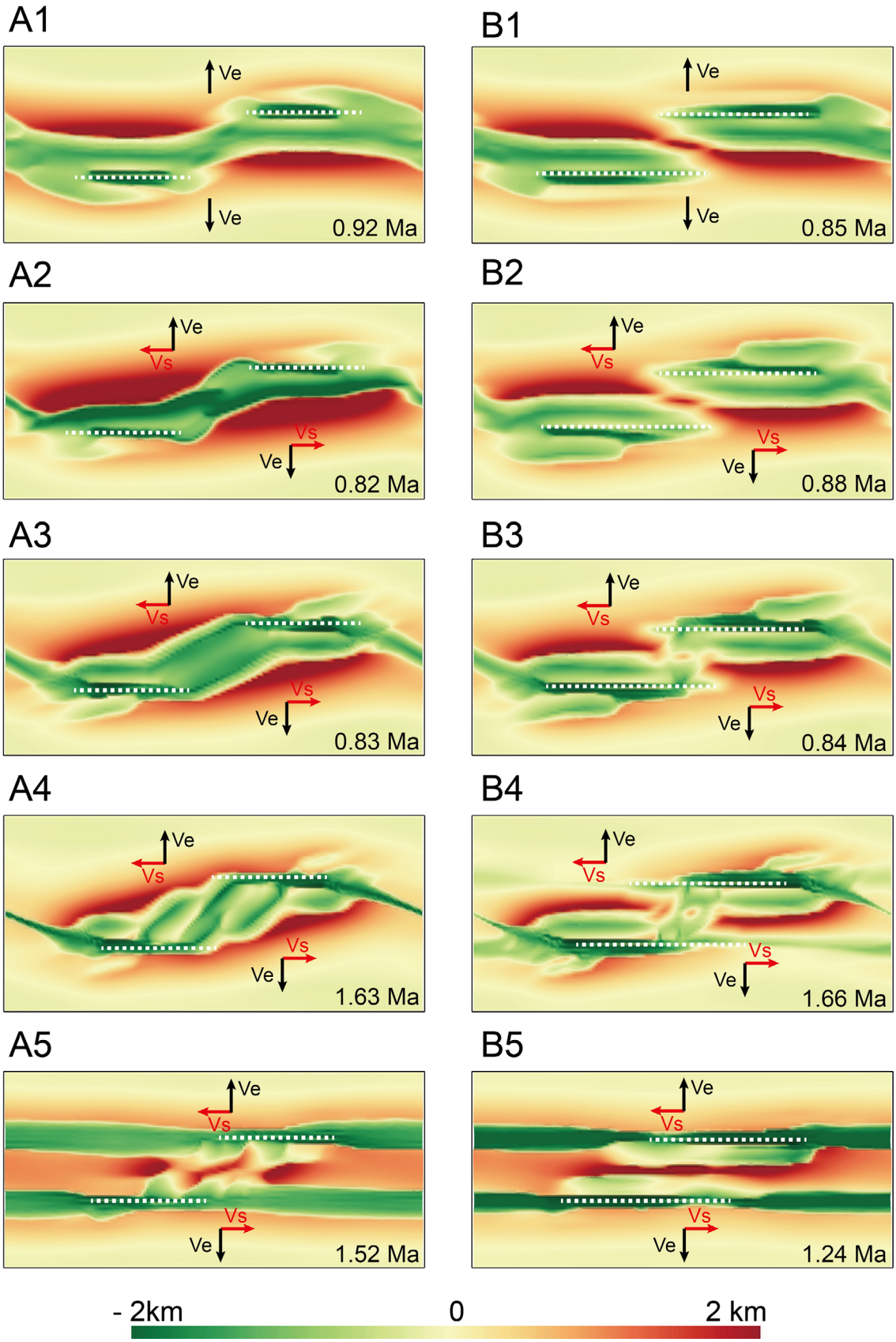

Fig. 5. The surface relief influenced by different ratios of extension rate to shear rate applied and the spatial relationship of faults. The first and second columns correspond to the standard models: Models A and B (Fig. 3), respectively. Pre-existing faults are indicated in white dotted lines. Boundary conditions are indicated by black and red arrows.

https://doi.org/10.1007/s12303-018-0057-5

Experiments A5 and B5 were designed to have a ratio of 0.25 (extension rate to shear rate). This indicates that the fault system is dominated by the tangential component of velocity boundary conditions. Two subsidence belts are observed along the strike of pre-existing faults, yielding a subsidence of about 1.5–2 km at 1.5 Ma. The uplifted regions are observed mainly between the two subsidence belts, as well as slightly along the external boundaries of the subsidence belts. In experiment A5, the uplifted region between the two subsidence belts shows a step form (Fig. 5A5), while in Experiment B5 it displays a linear distribution of uplifted area (Fig. 5B5). The two experiments yield a similar uplift of about 2km.

4.3. Particles Motion: Extension versus Transtension

Here, to compare and quantify the effect of boundary conditions on the lower crust exhumation and the compensation from the upper mantle to the overlying crust (crustal thinning during extension), two groups of passive particles are positioned (Figs. 6 and 7) at the upper surfaces of the lower crust, and another set at the Moho, respectively.

In extension (experiment B1, Table 1), no significant exhumation (Fig. 6) is observed prior to 0.25 Ma, and the compensation from the upper mantle to the overlying crust is not remarkable, either. At about 0.85 Ma, a maximum uplift of about 10 km

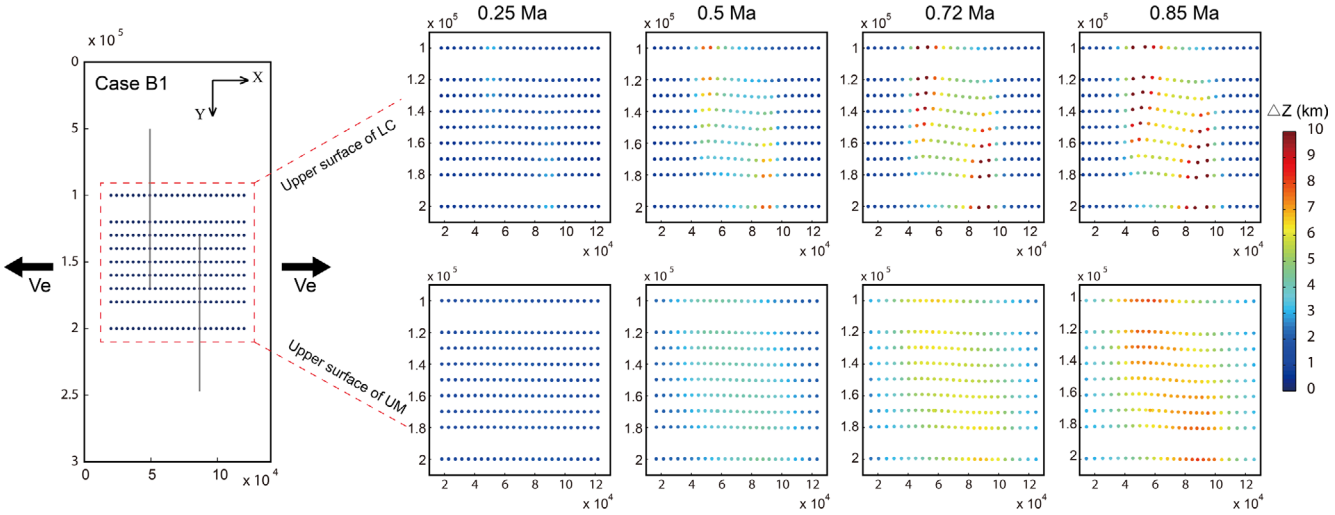

Fig. 6. Model B1: evolution of migration of passive particles during extension. In left panel, the coordinate system is identical to Figure 3. The upper surfaces of the lower crust (LC, upper panel) and the upper mantle (UM, lower panel) contain 450 passive particles in total. The exhumation of passive particles is shown by the colour bar. Two pre-existing faults are indicated in black lines in left panel. Extension boundary conditions are indicated in black arrows.

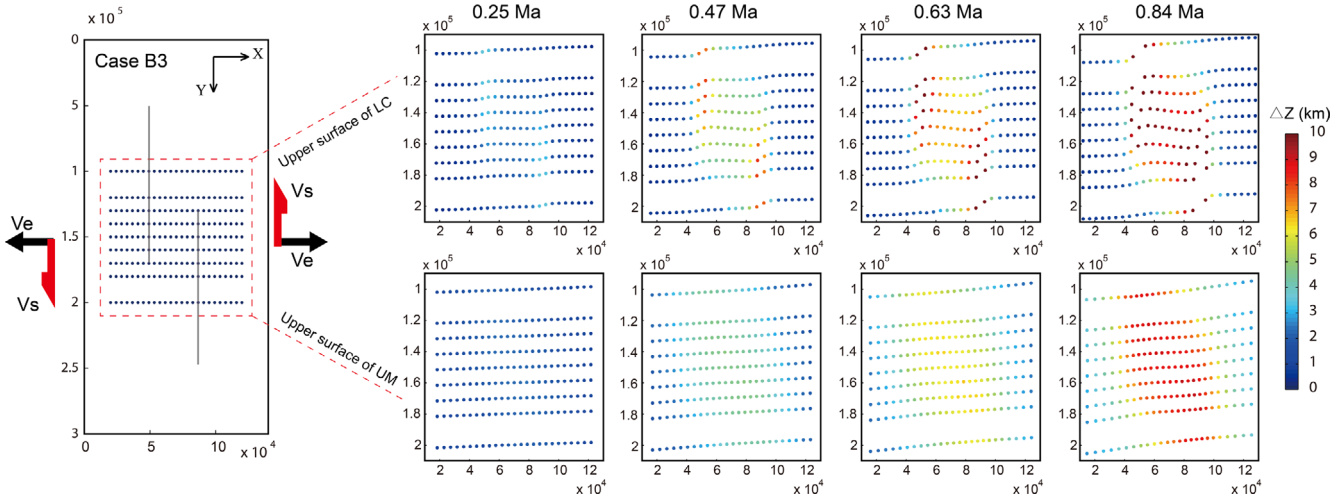

Fig. 7. Model B3, migration of passive particles during transtension. 450 particles divided into two groups are placed in the upper surfaces of the lower crust (LC) and the upper mantle (UM), respectively. The colour of passive particles represents the exhumation of the lower crust and the compensation from the upper mantle to the overlying crust during transtension. Two vertical faults are placed (black lines in left panel). Boundary conditions are shown by red and black arrows. Vs and Ve with red and black arrows represent the rates and directions of shear and extension (see detailed parameters in Table 1), respectively.

(dark red in Fig. 6) is recorded by the particles placed along faults, while the particles in the relay zone between faults only show about 6 km of uplift (yellow to light orange colour in Fig. 6). With respect to the deeper particles placed at the Moho, they yield a maximum uplift of about 6–7 km, showing a similar distribution with the uplifted regions observed in the upper particles.

In transtension (experiment B3), all the particles move and rotate (non uniform rate) with the applied tangential component of velocity boundary conditions (Fig. 7). The distribution of uplift does not show significant difference compared to experiment B1 (extension) prior to about 0.47 Ma. As transtension continues (at about 0.63 Ma), the upper particles located in the relay zone between faults significantly exhume, yielding a height of about 7 km. At about 0.84 Ma, the upper particles record a maximum uplift of about 10 km. With respect to the particles placed at the Moho, they show a relatively even distribution of uplift, yielding a height of about 8–9 km at 0.84 Ma (9.52~10.71 km/Ma).

5. DISCUSSION

5.1. Migration of Particles: Extension versus Transtension

In a system comprised of pre-existing faults and partially molten lower crustal rocks, the orientation of faults and boundary conditions are both thought to play an important role in influencing the distribution of lower crust exhumation (Rey et al., 2009). Their results show that the passive particles in the middle plane integrally move towards the intersection zones of pre-existing faults and largely contribute to regional exhumation.

The uplift observed on the deeper particles can be explained by the isostatic (airy mode) compensation from the lower density mantle to the thinning part of overlying crust during transtension (Abers et al., 2002). The difference in uplift between the two planes of particles (the upper surfaces of the lower crust and the upper mantle) is about 3–4 km under extension (case B1) and ~1–2 km under transtension (case B3), respectively (Figs. 6 and 7). The reason for forming such gap of uplift between the upper and lower planes of particles is probably due to (1) the partially molten rocks in the middle level of the lower crust significantly move towards the relay zone between faults, and make a significant contribution to regional exhumation, (2) the upper mantle rocks are mechanically stronger compared to the lower crust rocks (partially molten rocks) and they must show more resistance to deformation compared to the overlying partially molten lower crust and display some lag to flow upward to compensate the thinning part of the overlying crust (Abers et al., 2002; Piccardo, 2016). This also indicates that, for experiment B1 controlled by extension, the partially molten lower crustal rocks in the middle level make a higher contribution to exhumation in the relay zone between faults than that under transtension (experiment B3). In other words, the low-density upper mantle compensates much more the overlying crust in experiment B3 (transtension) compared to experiment B1 (extension). This inference is supported by the plots of the exhumation rate over time in Figures 8a and 9a (detail in section 5.2).

According to the distribution of upwelling partially molten rocks observed in experiments B1 and B3, the regional exhumation of the lower crust along the faults does not show significant difference between the cases in extension and transtension. In the relay zone between faults, the tangential component of velocity boundary conditions plays an important role in concentrating partially molten rocks. The reason for focusing of the partially molten rocks in the relay zone is probably due to the tangential component of velocity boundary conditions that also link damage/weak zones (Kim et al., 2004) around a strike-slip fault zone. The linking damage/weak zones evolve and become matured through the interaction between the tips of adjacent faults (Kim et al., 2001), undergoing a process from a soft linkage to a hard linkage. These damage/weak zones (in the relay zone between faults) could make a direct contribution to concentrating partially molten rocks during transtension (extension), this process could be also indirectly assisted and enhanced by the removal of overburden in the relay zone (subsidence regions shown in Fig. 5).

5.2. Exhumation Rate

Here, we discuss the influence of the spatial relationship of faults and ratio of extension rate to shear rate applied on boundaries on exhumation rate of the partially molten lower crust rocks.

Figures 8a and 9a show the vertical velocity (time dependent) of a selected particle (its coordinate: (70, 150, –32) /km, Fig. 3) pertaining to the upper surface of the lower crust, which can be used to indicate the exhumation rate of the partially molten lower crustal materials during transtension (extension). During extension/transtension, rocks can be transferred from the underlying low-density mantle to the overlying crust (crustal thinning) due to isostatic imbalance, this is referred to a compensation process (Banks et al., 1977). Figures 8b and 9b present the vertical velocity (time dependent) of a passive particle (its coordinate: (70, 150, –42) /km, Fig. 3) initialized in the upper surface of the upper mantle, which can be employed to quantify the compensated process occurred in the relay zone between faults.

For Models A and B, the compensation rate from the upper mantle to the overlying crust generally shows a similar trend with the exhumation rate of the lower crust (Figs. 8 and 9). At the ratio of 1 (extension rate equals shear rate), the maximum

https://doi.org/10.1007/s12303-018-0057-5

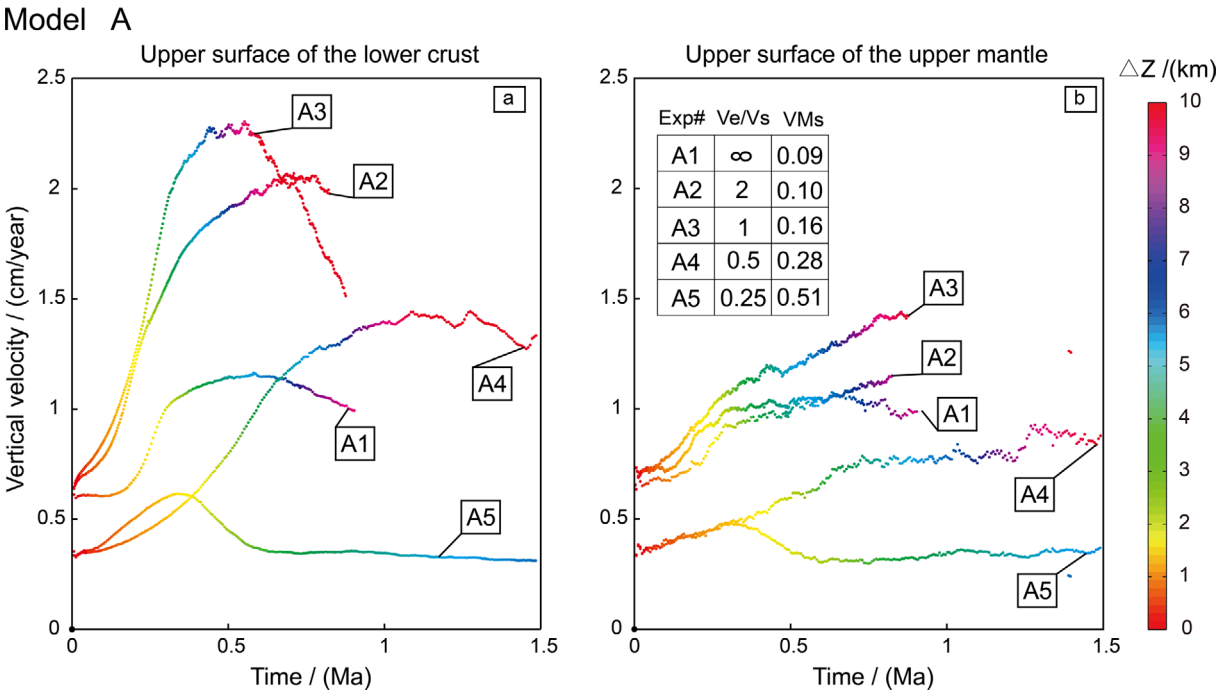

Fig. 8. Model A. (a) Exhumation rate of the lower crust, (b) the isostatic compensation from the upper mantle to the overlying crust. The passive particles employed for plotting the left and right figures are located at (70, 150, –32) and (70, 150, –42) (/km), respectively. The colour bar represents the accumulative height of exhumation over time. Exp# is the name of experiment. Ve/Vs is the ratio of extension rate to shear rate applied on the boundaries. VMs represents the Von Mises equivalent strain.

rate of the lower crust exhumation is observed in the relay zone between faults, as well as the maximum compensation rate from the upper mantle to the overlying crust. When the ratio of extension rate to shear rate was set to 0.25, indicating a predominantly simple shear fault system, the lowest rates of the exhumation and the compensation are recorded in the relay zone.

In terms of the influence of spatial relationship of pre-existing faults on the lower crust exhumation and the compensation from the upper mantle to the overlying crust (Models A with B, Figs. 8 and 9), Model A (experiments A1–A4) generally shows a high exhumation rate compared to Model B (experiments B1–B4). This indicates that the relay zone between faults in Model A prefers to concentrate the partially molten lower rocks compared to Model B (Fig. 3). Experiments A5 and B5 having a ratio of 0.25 (extension rate to shear rate) do not show significant difference in the vertical velocity (Figs. 8 and 9). In addition, the curves in Model A show a generally linear increase of vertical velocity over time prior to arriving about 10 km of uplift (Fig. 8). For Model B, some early peaks of vertical velocity are observed at about 0.3 Ma (Fig. 9).

The difference in the paths of capturing vertical velocity between Models A and B probably suggests a different process of developing high strain zones and exhuming the partially molten lower crust exhumation took place in the relay zone between faults during extension and transtension. Since the pure extensional cases (experiments A1 and B1) do not show significant exhumation in the relay zone between faults (Figs. 4A1 and 4B1), we thereby only focus on discussing the developmental process of the lower crust exhumation under transtension (experiments A2–A5 and B2–B5).

We here suggest a conceptual model (Fig. 10) to explain the possible mechanisms that result in appearing early vertical velocity peaks in Figure 9. In order to locate the faults, we employed nodes m, n, p and q to describe the faults. At a fault tip, it commonly has a maximum stress concentration (e.g., Cowie and Scholz, 1992; Gupta and Scholz, 2000). The interaction between the tips of faults leads to the growth, propagation and maturation of faults (Kim et al., 2001).

In Model A (Fig. 10), nodes n and p (tips of faults) must intensely interact with a high stress concentration (e.g., Soliva et al., 2008) resulting in linking each other through fractures (Kim et al., 2001, 2004; Mukherjee, 2019) when they are initially re-activated. After the re-activation, we can ideally mark the linked fractures (blue line in Fig. 10) according to the analogue (Peacock and Parfitt, 2002; Bellahsen and Deniel, 2005), numerical modelling (Soliva et al., 2008) and field investigations (Hus et al., 2006; Giba et al., 2012). The linked high strain zones are generally sub-orthogonal to the equivalent direction of transtension (red arrows in Fig. 10). In other words, these high strain zones would be fully stretched over time by the equivalent transtensional boundary.

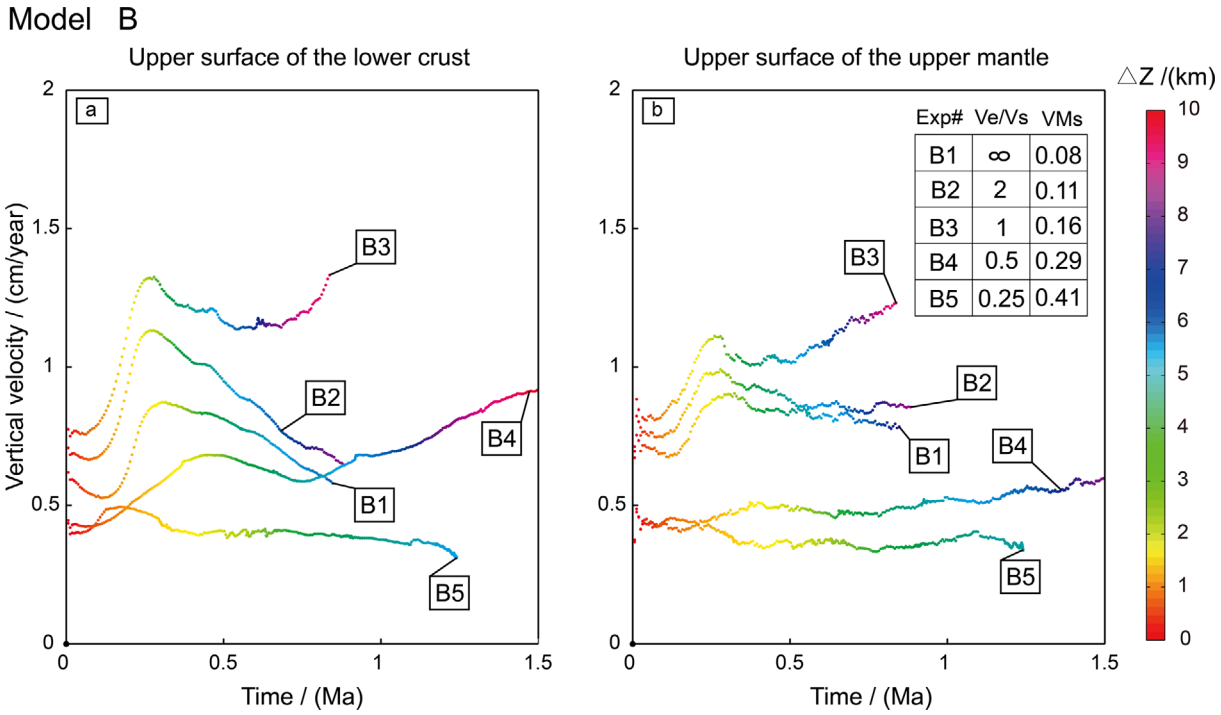

Fig. 9. Model B. (a) Exhumation rate of the lower crust, (b) the isostatic compensation from the upper mantle to overlying crust. The passive particles employed for plotting (a) and (b) are located at (70, 150, –32) and (70, 150, –42) (/km), pertaining to the upper surfaces of the lower crust and the upper mantle, respectively.

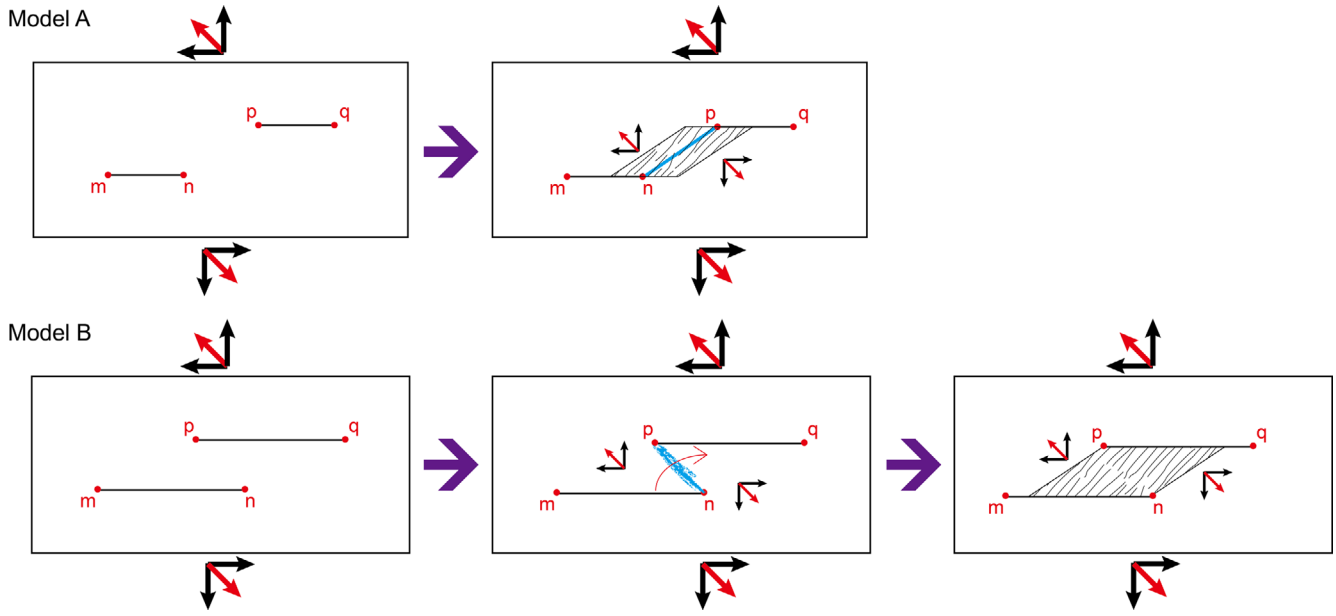

Fig. 10. Conceptual models are constructed to explain the process of faults-related exhumation in the overlapping zone. The first column shows the initial geometry of pre-existing faults according to the numerical model setup (Models A and B, from Fig. 3), m, n, p and q are used to mark the tips of faults. Black arrows represent the applied extension and shear rates, red arrows represent the equivalent direction of transtension. The middle and right columns represent the different stages of producing linking high strain zones driven by the external boundary conditions.

This indicates that the partially molten lower crust beneath the relay zone between faults would sub-linearly exhume (as shown in Fig. 8) to the middle–upper crust along the blue line and its surrounding areas (indicated by inclined black lines, Fig. 10). This conclusion can be evidenced by both the spatial distribution (Fig. 4) and the sub-linear exhumation rate (Fig. 8) of the partially molten lower crust.

In terms of Model B, nodes n and p would undergo the same

https://doi.org/10.1007/s12303-018-0057-5

processes (concentrating high stress; e.g., Cowie and Scholz, 1992; Gupta and Scholz, 2000) with Model A when they are initially re-activated. The strike of the linked high strain zones (blue line in Model B, Fig. 10) would be sub-parallel to the equivalent direction of transtension. This indicates that the linked high strain zones are not predominant sites (blue line of Model B) to concentrate strain over time in transtension. We propose that the linked high strain zones resulted from the initial re-activation (blue line in Model B, Fig. 10) would be reprinted and overlapped during transtension (Kim et al., 2001). This probably can help explain the early peaks of vertical velocity observed in Model B (Fig. 9). In addition, this conceptual model also indicates that the newly produced high strain zones (indicated by inclined lines, Fig. 10) would be generally sub-orthogonal to the equivalent direction of transtension. Partially molten lower crust rocks would exhume along the strike of the newly produced high strain zones. This feature coincides well with our numerical results (Fig. 4), showing that the strike of the exhumation belt (red) made of the partially molten lower crust in the relay zone between faults is sub-orthogonal to the equivalent direction of transtension.

5.3. Model Implications for the Ghanaian Sefwi Terrane

Craton-scale shear zones in NW Ghana (Block et al., 2015) and SW (McFarlane et al., 2016) commonly mark the boundaries between low-grade greenstone belts and high-grade metamorphic rocks of up to amphibolite–migmatite facies. Identifying the role the shear zones play in the exhumation of the lower crust in Birimian province can allow to better understand the evolution of deformation during the Eburnean Orogeny (ca. 2.2–2.0 Ga).

In the Sefwi terrane, the high grade tectono-metamorphic KJD is bounded by two main shear zones: the Ketesso and Kenyase shear zones. Based on the fault-induced exhumation of the lower crust shown by the numerical results (Fig. 11a), the western boundary (red dotted line, Fig. 11a) bounding the lower

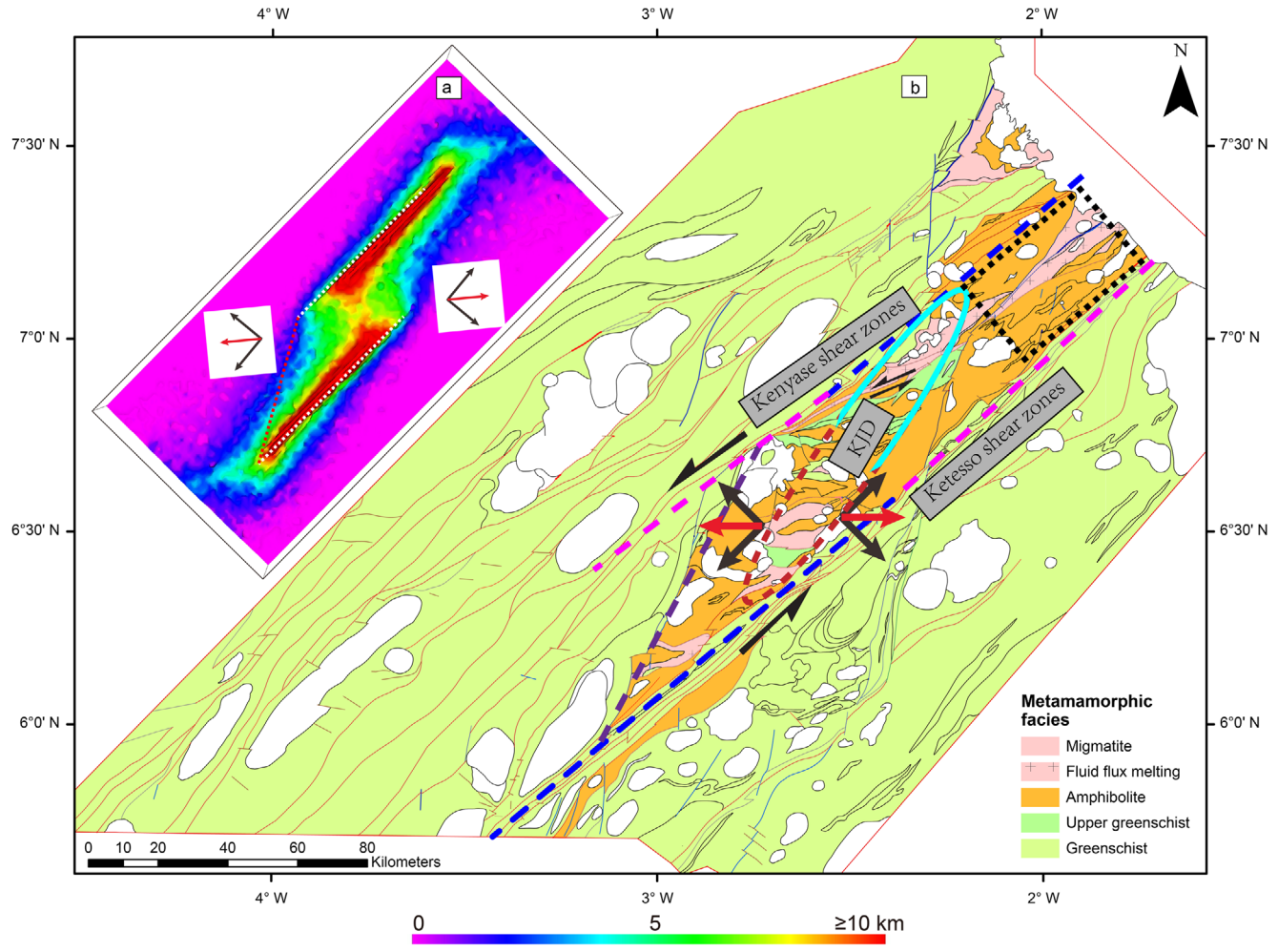

Fig. 11. (a) The numerical results (case B3, Fig. 4B3) show the uplift of the upper surface of the partially molten lower crust (0–10 km scale colour bar). (b) Metamorphic map in the Sefwi terrane modified after McFarlane (2018). Transtension boundary conditions are indicated by red arrows.

crustal materials is sub-parallel to the exhumation belt (red belt) in the relay zone between faults, and is sub-orthogonal to the equivalent direction of transtension (red arrows in Fig. 11a). This feature coincides well with the metamorphic map in the Sefwi terrane (McFarlane, 2018), the western boundary (purple dotted line in Fig. 11b) of the KJD is sub-parallel to the distribution of migmatite (indicated by ellipse) and sub-orthogonal to the ENE-WSW transtension direction.

The concentration of the partially molten lower crust rocks increases along the direction from the relay zone to fault tips (Fig. 11a). This can be used to explain the distribution of the migmatite–amphibolite bounded by an ellipse in the KJD in field, with a high concentration of migmatite around the heads of the ellipse (red and light blue areas, Fig. 11b) and of amphibolite in the central part of the ellipse.

Regarding the evolution of structures, we suggest that the Ketesso and Kenyase shear zones probably underwent two stages for growth and maturation from the D1 to D2 deformation phases. During the D1 compression stage, the preliminary structures of the two shear zones were initialized in parallel. The Ketesso shear zones did not cross through the Sefwi terrane during the D1 stage, and they were located only in the southern part of the Sefwi terrane (dark blue dotted line, Fig. 11b). At the same time, the preliminary forms of the Kenyase shear zones were located only in the northern part of the Sefwi terrane (dark blue dotted line, Fig. 11b). This distribution of the two shear zones probably resulted from a significantly oblique component of the D1 compression stage. These preliminary structures of the Ketesso and Kenyase shear zones provided preferential sites for subsequent re-activation. During the subsequent D2 transtension, the two shear zones developed along their initial strikes (pink dotted lines) and became matured.

With respect to the high-grade rocks observed in the North-Eastern part of the Sefwi terrane (indicated by black dotted box, Fig. 11b), if we accept this model, this could be explained by regional exhumation controlled and promoted by the newly matured part (pink dotted part, Fig. 11b) of the Ketesso shear zones during the D2 transtension. Second-order faults between the two main shear zones (the Ketesso and Kenyase shear zones) could also have made a significant contribution to the exhumation of the high-grade rocks.

Regarding the time length required for the regional exhumation of the partially molten lower crust (~10 km of uplift equalling to a drop in pressure of 4 kbar during the D2 transtension stage suggested by McFarlane et al., 2016), according to our numerical experiments, all the modelling results yield a similar time length of less than 2 Ma when using rates of 1–2 cm/year for extension and 0–4 cm/year for simple shear. Considering the variations in velocities (Vs and Ve) applied on boundaries, we suggest that the main regional exhumation of the lower crust in the Sefwi terrane probably occurred within a short duration of < 5 Ma.

5.4. Limitations and Perspectives

Although we have tested ten 3D thermo-mechanical models under extension and transtension boundary conditions, the ratio of extension rate to shear rate applied on boundaries should be more extensively tested in further models. In our study, we focused our attentions on exploring the regional exhumation of the lower crust exhumation influenced by the spatial relationship of pre-existing faults and boundary conditions. But the process of fluid transfer in fractures/faults was thus deliberately not included. We aim to couple this process in future studies by employing solid-fluid mechanisms developed by Keller et al. (2013). Regarding the effective viscosity of partially molten rocks, it is still overestimated in this study compared to the experimental results (between 10^{6}–10^{18} Pa s; Vanderhaeghe, 2001). This is due to the high complexity in computing huge viscosity variations (Moresi and Solomatov, 1995).

We aim to improve the setup of the initial model (e.g., more realistic spatial-relationship of pre-existing faults, dating the timing of main structures in the study area) under the assistance of more field works in the future. In addition, we only concerned here the D2 deformation stage occurred in the Sefwi terrane of SW Ghana. We installed the initial model according to the geological data estimated at the end of the D1 deformation stage (P, T and crustal thickness based on the metamorphic estimates performed by Block et al. (2015) and McFarlane et al. (2016)). In particular, the variation in the distribution of the Moho depth (Jessell et al., 2016) resulting from the D1 compression stage was not taken into considerations for modelling. That could be interesting if we can perform a continuous process for the Sefwi terrane by including the D1 crustal thickening (Feng et al., 2016a, 2016c) and the D2 transtension triggering the regional exhumation. In addition, we aim to involve more geophysical and geochemical constrains (Ganne et al., 2016; Mukherjee, 2017b, 2018b) to improve the model setup (e.g., geochronological data; density variation, more P-T paths; distribution of Moho depth; thickness of the lithosphere and the mantle potential temperature during the Eburnean Orogeny etc.).

Regarding the investigated development of the Montagne Noire MCC in the French Massif Central by Echtler and Malavieille (1990), it was related with process of crustal extension/transtension and thinning during the collapse. The extensional/transtensinoal process formed steeply dipping normal and strike-slip faults, allowing the uplift. This uplift was dominantly contributed by the exhumation of HT migmatite and anatectic granite. The formation of the MCC in the Variscan belt suggests that the

https://doi.org/10.1007/s12303-018-0057-5

extensional/transtensional evolution influenced all the metamorphic process and areas.

6. CONCLUSIONS

In this study, we constructed ten 3D thermo-mechanical model to test the role pre-existing faults and boundary conditions that play in the exhumation of the lower crust. Different patterns of faults and boundary conditions were tested.

The 3D models show that the normal component of boundary conditions in the fault system controls the exhumation of the lower crust along faults, while the exhumation in the relay zone between faults is dominated by the ratio of extension rate to shear rate applied on boundaries. The strike of the exhumation belt made of partially molten lower crustal materials in the relay zone between faults is sub-orthogonal to the transtension direction. The spatial relationship of faults controls the distribution of surface relief in general. The maximum subsidence and uplift yield relief values of about –2 km and 2 km, respectively. The isostatic compensation from the low-density upper mantle to the overlying crust (crustal thinning) is higher under transtension than that under extension.

The exhumation of the partially molten lower crust rocks controlled by high strain zones can be used to better understand the loci of the high-grade rocks in the Sefwi terrane. The KJD comprised of up to amphibolite–migmatite facies probably resulted from the concentration of the partially molten rocks in the relay zone between the Ketesso and Kenyase shear zones during the D2 ENE-WSW transtension (a drop in pressure of about 4 kbar). These two shear zones could undergo two phases for development and growth from the D1 to D2 deformation stages. The mainly regional exhumation in the Sefwi terrane probably occurred within a duration of less than 5 Ma.

ACKNOWLEDGMENTS

This research was funded by the Fundamental Research Funds for the Central Universities grant number 2018QNB01. Helen McFarlane is greatly thanked for fruitful discussions on this paper and providing us the metamorphic maps of SW Ghana. Patrice Rey, Loïc Labrousse and Prince Amponsah are greatly thanked for comments on the earlier version of this paper. The editor and Soumyajit Mukherjee are warmly thanked for very constructively reviewing the paper.

REFERENCES

Abers, G.A., Ferris, A., Craig, M., Davies, H., Lerner-Lam, A.L., Mutter, J.C., and Taylor, B., 2002, Mantle compensation of active metamorphic core complexes at Woodlark rift in Papua New Guinea. Nature, 418, 862–865.

Agyei Duodu, J., Loh, G.K., and Boamah, K.O., 2009, Geological map of Ghana (1:1,000,000). Geological Survey Department of Ghana (GSD).

Baratoux, L., Metelka, V., Naba, S., Jessell, M.W., Grégoire, M., and Ganne, J., 2011, Juvenile Paleoproterozoic crust evolution during the Eburnean orogeny (~2.2–2.0 Ga), western Burkina Faso. Precambrian Research, 191, 18–45.

Banks, R.J., Parker, R.L., and Huestis, S.P., 1977, Isostatic compensation on a continental scale: local versus regional mechanisms. Geophysical Journal International, 51, 431–452.

Bellahsen, N. and Daniel, J.M., 2005, Fault reactivation control on normal fault growth: an experimental study. Journal of Structural Geology, 27, 769–780.

Block, S., Ganne, J., Baratoux, L., Zeh, A., Parra-Avila, L.A., Jessell, M., Ailleres, L., and Siebenaller, L., 2015, Petrological and geochronological constraints on lower crust exhumation during Paleoproterozoic (Eburnean) orogeny, NW Ghana, West African Craton. Journal of Metamorphic Geology, 33, 463–494.

Brun, J.P., Sokoutis, D., and Van Den Driessche, J., 1994, Analogue modeling of detachment fault systems and core complexes. Geology, 22, 319–322.

Chester, J.S., Logan, J.M., and Spang, J.H., 1991, Influence of layering and boundary conditions on fault-bend and fault-propagation folding. Geological Society of America Bulletin, 103, 1059–1072.

Cowie, P.A. and Scholz, C.H., 1992, Physical explanation for the displacement-length relationship of faults using a post-yield fracture mechanics model. Journal of Structural Geology, 14, 1133–1148.

Dasgupta, S. and Mukherjee, S., 2017, Brittle shear tectonics in a narrow continental rift: asymmetric non-volcanic Barmer basin (Rajasthan, India). The Journal of Geology, 125, 561–591.

Drucker, D.C. and Prager, W., 2013, Soil mechanics and plastic analysis or limit design. Quarterly of Applied Mathematics, 10, 157–165.

Dooley, T.P. and Schreurs, G., 2012, Analogue modelling of intraplate strike-slip tectonics: a review and new experimental results. Tectonophysics, 574, 1–71.

Echtler, H. and Malavieille, J., 1990, Extensional tectonics, basement uplift and Stephano-Permian collapse basin in a late Variscan metamorphic core complex (Montagne Noire, southern Massif Central). Tectonophysics, 177, 125–138.

Faulkner, D.R., Jackson, C.A.L., Lunn, R.J., Schlische, R.W., Shipton, Z.K., Wibberley, C.A.J., and Withjack, M.O., 2010, A review of recent developments concerning the structure, mechanics and fluid flow properties of fault zones. Journal of Structural Geology, 32, 1557–1575.

Feng, X., Amponsah, P.O., Martin, R., Ganne, J., and Jessell, M.W., 2016a, 3-D numerical modelling of the influence of pre-existing faults and boundary conditions on the distribution of deformation: example of North-Western Ghana. Precambrian Research, 274, 161–179.

Feng, X., Jessell, M.W., Amponsah, P.O., Martin, R., Ganne, J., Liu, D., and Batt, E.G., 2016b, Effect of strain-weakening on Oligocene-Miocene self-organization of the Australian-Pacific plate boundary fault in southern New Zealand: insights from numerical modelling. Journal of Geodynamics, 100, 130–143.

Feng, X., 2016c, Modélisation numérique des failles décrochantes et des effets de compression grande échelle – Cas d'étude en Afrique de l'Ouest et Nouvelle Zélande. Ph.D. Thesis, Universit de Toulouse, Universit Toulouse III-Paul Sabatier, Toulouse, 230 p.

Feybesse, J.L., Billa, M., Guerrot, C., Duguey, E., Lescuyer, J.L., Milesi, J.P., and Bouchot, V., 2006, The paleoproterozoic Ghanaian province: geodynamic model and ore controls, including regional stress modeling. Precambrian Research, 149, 149–196.

Fossen, H. and Tikoff, B., 1998, Extended models of transpression and transtension, and application to tectonic settings. In: Holdsworth, R.E., Strachan, R.A., and Dewey, J.F. (eds.), Continental Transpressional and Transtensional Tectonics. Geological Society, London, Special Publications, 135, p. 15–33.

Ganne, J., De Andrade, V., Weinberg, R.F., Vidal, O., Dubacq, B., Kagambega, N., Naba, S., Baratoux, L., Jessell, M., and Allibon, J., 2012, Modern-style plate subduction preserved in the Palaeoproterozoic West African craton. Nature Geoscience, 5, 60–65.

Ganne, J., Gerbault, M., and Block, S., 2014. Thermo-mechanical modeling of lower crust exhumation – constraints from the metamorphic record of the Palaeoproterozoic Eburnean orogeny, West African Craton. Precambrian Research, 243, 88–109.

Ganne, J., Feng, X., Rey, P., and Andrade, V.D., 2016, Statistical petrology reveals a link between supercontinents cycle and mantle global climate. American Mineralogist, 101, 2768–2773.

Gerya, T.V., Perchuk, L.L., and Burg, J.P., 2008, Transient hot channels: perpetrating and regurgitating ultrahigh-pressure, high-temperature crust-mantle associations in collision belts. Lithos, 103, 236–256.

Giba, M., Walsh, J.J., and Nicol, A., 2012, Segmentation and growth of an obliquely reactivated normal fault. Journal of Structural Geology, 39, 253–267.

Gueydan, F., Précigout, J., and Montesi, L.G., 2014, Strain weakening enables continental plate tectonics. Tectonophysics, 631, 189–196.

Gupta, A. and Scholz, C.H., 2000, A model of normal fault interaction based on observations and theory. Journal of Structural Geology, 22, 865–879.

Hirdes, W., Davis, D.W., and Eisenlohr, B.N., 1992, Reassessment of Proterozoic granitoid ages in Ghana on the basis of U/Pb zircon and monazite dating. Precambrian Research, 56, 89–96.

Hus, R., De Batist, M., Klerkx, J., and Matton, C., 2006, Fault linkage in continental rifts: structure and evolution of a large relay ramp in Zavarotny; Lake Baikal (Russia). Journal of Structural Geology, 28, 1338–1351.

Jessell, M.W., Amponsah, P.O., Baratoux, L., Asiedu, D.K., Loh, G.K., and Ganne, J., 2012, Crustal-scale transcurrent shearing in the Paleoproterozoic Sefwi-Sunyani-Como region, West Africa. Precambrian Research, 212–213, 155–168.

Jessell, M.W., Begg, G.C., and Miller, M.S., 2016, The geophysical signatures of the West African Craton. Precambrian Research, 274, 3–24.

Keller, T., May, D.A., and Kaus, B.J., 2013, Numerical modelling of magma dynamics coupled to tectonic deformation of lithosphere and crust. Geophysical Journal International, 195, 1406–1442.

Kim, Y.S., Andrews, J.R., and Sanderson, D.J., 2001, Reactivated strike-slip faults: examples from north Cornwall, UK. Tectonophysics, 340, 173–194.

Kim, Y.S., Peacock, D.C., and Sanderson, D.J., 2004, Fault damage zones. Journal of Structural Geology, 26, 503–517.

Koyi, H.A. and Skelton, A., 2001, Centrifuge modelling of the evolution of low-angle detachment faults from high-angle normal faults. Journal of Structural Geology, 23, 1179–1185.

Le Pourhiet, L., Burov, E., and Moretti, I., 2004, Rifting through a stack of inhomogeneous thrusts (the dipping pie concept). Tectonics, 23. https://doi.org/10.1029/2003TC001584

Lin, C.H., 2000, Thermal modeling of continental subduction and exhumation constrained by heat flow and seismicity in Taiwan. Tectonophysics, 324, 189–201.

Lin, S., Jiang, D., and Williams, P.F., 1998, Transpression (or transtension) zones of triclinic symmetry: natural example and theoretical modelling. In: Holdsworth, R.E., Strachan, R.A., and Dewey, J.F. (eds.), Continental Transpressional and Transtensional Tectonics. Geological Society, London, Special Publications, 135, p. 41–57.

McFarlane, H.B., Block, S., Ailleres, L., Betts, P., Ganne, J., Baratoux, L., and Jessell, M., 2016, Lower and middle crust exhumation during Palaeoproterozoic accretionary tectonics: key new evidence from the Sefwi Greenstone Belt, SW Ghana. Proceedings of the 35th International Geological Congress (Abstract), Aug. 27–Sep. 4, Cape Town, p. 4504.

McFarlane, H.B., 2018, The geodynamic and tectonic evolution of the Palaeoproterozoic Sefwi Greenstone Belt, West African Craton (Ghana). Ph.D. Thesis, Universit Toulouse 3 Paul Sabatier (UT3 Paul Sabatier) et Monash University (Australie), Toulouse, 297 p.

Milési, J.P., Feybesse, J.L., and Pinna, P., 2004, Geological map of Africa (1:10,000,000), SIGAfrique project. Proceedings of the 20th Conference of African Geology, Orleans, Jun. 2–7. Available at: http://www.sigafrique.net

Misra, A.A. and Mukherjee, S., 2015, Tectonic Inheritance in Continental Rifts and Passive Margins. Springer International Publishing, Cham, 88 p.

Moresi, L. and Solomatov, S., 1995, Numerical investigation of 2D convection with extremely large viscosity variations. Physics of Fluids, 7, 2154–2162.

Moresi, L., Dufour, F., and Mühlhaus, H.B., 2003, A Lagrangian integration point finite element method for large deformation modeling of viscoelastic geomaterials. Journal of Computational Physics, 184, 476–497.

Moresi, L., Quenette, S., Lemiale, V., Meriaux, C., Appelbe, B., and Muhlhaus, H., 2007, Computational approaches to studying non-linear dynamics of the crust and mantle. Physics of the Earth and Planetary Interior, 163, 69–82.

Morley, C.K., Haranya, C., Phoosongsee, W., Pongwapee, S., Kornsawan, A., and Wonganan, N., 2004, Activation of rift oblique and rift parallel pre-existing fabrics during extension and their effect on deformation style: examples from the rifts of Thailand. Journal of Structural Geology, 26, 1803–1829.

Mukherjee, S. and Mulchrone, K., 2012, Estimating the viscosity and Prandtl number of the Tso Morari Gneiss Dome, western Indian Himalaya. International Journal of Earth Sciences, 101, 1929–1947.

Mukherjee, S., 2013, Channel flow extrusion model to constrain dynamic viscosity and Prandtl number of the Higher Himalayan Shear Zone. International Journal of Earth Sciences 102, 1811–

1835.
Mukherjee, S., 2017a, Shear heating by translational brittle reverse faulting along a single, sharp and straight fault plane. Journal of Earth System Science, 126. https://doi.org/10.1007/s12040-016-0788-5
Mukherjee, S., 2017b, Airy's isostatic model: a proposal for a realistic case. Arabian Journal of Geosciences, 10, 268. https://doi.org/10.1007/s12517-017-3050-9
Mukherjee, S., 2018a, Locating center of gravity in geological contexts. International Journal of Earth Sciences, 107, 1935–1939.
Mukherjee, S., 2018b, Moment of inertia for rock blocks subject to bookshelf faulting with geologically plausible density distributions. Journal of Earth System Science, 127, 80. https://doi.org/10.1007/s12040-018-0978-4
Mukherjee, S., 2019, Using graph theory to represent fracture networks. In: Billi, A. and Fagereng, A. (eds.), Problems and Solutions in Structural Geology and Tectonics. Developments in Structural Geology and Tectonics Series, v. 5. Elsevier, ISBN: 9780128140482.
Pachell, M.A. and Evans, J.P., 2002, Growth, linkage, and termination processes of a 10-km-long strike-slip fault in jointed granite: the Gemini fault zone, Sierra Nevada, California. Journal of Structural Geology, 24, 1903–1924.
Peacock, D.C.P. and Parfitt, E.A., 2002, Active relay ramps and normal fault propagation on Kilauea Volcano, Hawaii. Journal of Structural Geology, 24, 729–742.
Piccardo, G.B., 2016, Evolution of the lithospheric mantle during passive rifting: inferences from the Alpine-Apennine orogenic peridotites. Gondwana Research, 39, 230–249.
Ranalli, G., 1995, Rheology of the Earth. Springer, Cham, 413 p.
Rey, P.F., Teyssier, C., and Whitney, D.L., 2009, The role of partial melting and extensional strain rates in the development of metamorphic core complexes. Tectonophysics, 477, 135–144.
Rollinson, H., 2016, Archaean crustal evolution in West Africa: a new synthesis of the Archaean geology in Sierra Leone, Liberia, Guinea and Ivory Coast. Precambrian Research, 281, 1–12.
Sharples, W., Moresi, L.N., Jadamec, M.A., and Revote, J., 2015, Styles of rifting and fault spacing in numerical models of crustal extension. Journal of Geophysical Research: Solid Earth, 120, 4379–4404.
Soliva, R., Benedicto, A., Schultz, R.A., Maerten, L., and Micarelli, L., 2008, Displacement and interaction of normal fault segments branched at depth: implications for fault growth and potential earthquake rupture size. Journal of Structural Geology, 30, 1288–1299.
Teufel, L.W. and Clark, J.A., 1984, Hydraulic fracture propagation in layered rock: experimental studies of fracture containment. Society of Petroleum Engineers Journal, 24, 19–32.
Tirel, C., Brun, J.P., and Burov, E., 2004, Thermomechanical modeling of extensional gneiss domes. In: Whitney, D.L., Teyssier, C., and Siddoway, C.S. (eds.), Gneiss Domes in Orogeny. GSA Special Papers, Geological Society of America, 380, p. 67–78.
Tirel, C., Brun, J.P., and Burov, E., 2008, Dynamics and structural development of metamorphic core complexes. Journal of Geophysical Research: Solid Earth, 113. https://doi.org/10.1029/2005JB003694
Vanderhaeghe, O., 2001, Melt segregation, pervasive melt migration and magma mobility in the continental crust: the structural record from pores to orogens. Physics and Chemistry of the Earth, Part A: Solid Earth and Geodesy, 26, 213–223.